E.K. Njim[1], S.E. Sadiq[2], M.S. Al-Din Tahir[3], M.A. Flayyih[4], L. Hadji[5]

Flexural bending and fatigue analysis of functionally graded viscoelastic materials: experimental and numerical approaches

[1]*Ministry of Industry and Minerals, State Company for Rubber and Tires Industries, Iraq, emad.njim@gmail.com*
[2]*Department of Aeronautical Technical Engineering, Technical Engineering College of Najaf,*
Al-Furat Al-Awsat Technical University, Iraq
[3]*Department of Computer Engineering Technology, Faculty of Information Technology, Imam Ja'afar Al-Sadiq University, Iraq*
[4]*Biomedical Engineering Department, College of Engineering and Technologies, Al-Mustaqbal University, Hillah, Iraq*
[5]*Department of Mechanical Engineering, University of Tiaret, Tiaret, Algeria*

This work synthesized a thermoplastic polymer with varying densities along one direction using additive manufacturing technology to study the dynamic and static characteristics of functionally graded viscoelastic materials (FGVMs). To describe the mechanical properties of FGVMs, an analytical formulation based on the sigmoid-law formulation was proposed. The experimental program is conducted on 3D-printed samples, and various tests are conducted to examine the performance of such materials. Furthermore, the finite element method was used to evaluate the structural system's flexural properties. The influences of FG parameters and geometrical properties on flexural and reverse bending fatigue life are analyzed in detail. The results show that increasing porosity from 10% to 30% at a power-law index (k = 2) reduces bending strength by 31.25 percent and deflection by around 11.2 percent for VE samples. Changing the power-law exponent from 0.5 to 10 increases fatigue strength by 35 %.

Keywords: FGM, Polymeric materials, Mechanical Behavior, Fatigue, FEA.

Received 18 May 2023; Accepted 26 October 2023.

Introduction

FGMs can improve the performance of structures, especially when dealing with complex application environments. It is possible to avoid material delamination failures using these heterogeneous composite and reinforced materials [1]. Recently, FGMs have drawn considerable attention, and extensive research has been conducted on the mechanical behavior of such composites [2]. Developing FGMs with enhanced porosity and chemical composition will decrease defects caused by collisions between composites and structures [3].

The FGM design is often constructed of two materials and has varied material characteristics throughout the specified direction. Due to their exceptional properties, such as high-temperature resistance, excellent loading capacity, and extended fatigue life, FGM beams play an essential role in several unique applications. It can fully use its advantage by comprehending dimension and material mixing strategies that influence the performance and stability of FGM structures [4, 5]. An example of FGMs are structures made of functionally graded viscoelastic materials, which have many applications in contemporary engineering even though they present significant technical challenges in design and construction. Hence, many researchers were inspired by this to investigate the performance of FGVE structures using theoretical, numerical, and experimental techniques. The impacts of porosity distribution on the static and buckling properties of a functionally graded (FG) porous plate subjected to a transverse load were investigated using analytical and numerical analysis [6].

The quasi-static and dynamic compression of functionally graded (FG) metal syntactic has also been studied by Nima Movahedi et al. [7] using various experiments. Zhao Yin et al. conducted bending and free

vibration analyses of FGM porous plates using 3D elastic theory [8]. The bending problem of the VE beam was investigated and introduced by Ariza Gomez et al. [9], where specific essential characteristics were examined, such as material properties, load conditions, and structure arrangement.

The static, free vibration, and dynamic responses of a functionally graded piezoelectric material (FGPM) beam have also been investigated by M. Lezgy-Nazargah [10] using finite element analysis. The static analysis of power-law functionally graded plates was investigated by Mengzhen Li [11] with a novel generalized 5-unknown formulation.

A numerical solution for the analysis of viscoelastic FGM under finite strains is presented to study the extensive deformation analysis of viscoelastic functionally graded materials. [12]. Quansheng Zang et al. [13] examined the performance of FGM structures in static and free vibration analysis based on an isogeometrically scaled finite element method. The microstructure and properties of layered metal/rubber composites were studied by S.V. Kuteneva et al. [14]. In Shengwei Chen et al. [15], many experiments were performed to determine how impact characteristics affect a biomaterial composite made of a rigid 3D-printed beam and a soft viscoelastic foam used for protection. The finite element method (FEM) simulates the static and vibration properties of nonlinear viscoelastic sandwich beams made of viscoelastic materials [16]. Using the refined sinusoidal shear deformation beam theory, Zenkour et al. [17] employed the bending behavior of viscoelastic sandwich beams supported by elastic cores and resting on Pasternak's elastic foundations. The fatigue wear of a coating bonded to a rigid substrate based on two types of loads, constant and stochastically varying, is proposed by Stepanov and Torskaya [18]. More reports on static and free vibration analysis of functionally graded composite plates using various techniques have been investigated in some interesting references (see [19, 22]). Lihua Wang et al. [23] analyzed the static and dynamic problems of thin functionally graded shells (FGSs) with in-plane material inhomogeneity. Moreover, a novel nonlinear elasticity theory was applied to an annular or circular plate made from viscoelastic material. Because of this property, a uniformly loaded plate can experience large deformations [24]. Edouard et al. [25] proposed a new characterization method for 3D parametric lattice structures using FEM, driven by a design of experiments (DOE). Recently, Al-Hadrayi et al. [26] have presented numerical and experimental solutions to investigate fatigue behavior for Al/Zn using three types of FGM composite.

The literature reveals that many studies have explored the mechanical responses of FG structures involving porosity in recent years using numerical and analytical approaches. However, a few studies are related to the experimental work on fatigue and flexural analysis of FGVE beams. In this context, the paper investigates composite beams' mechanical properties and fatigue behavior that vary in stiffness through thickness using novel functionally graded porous polymeric materials.

In this study, the mechanical properties of FGVM were determined using a sigmoid function-based mathematical formula. The VE parameters are used in experiments to calculate banding and fatigue characteristics. Various properties are computed with Ansys software to verify experimental results following empirical findings. This paper is organized as follows: Section two depicts a mathematical formulation of porous FG beams. FEA is described in Section 3 to verify the results of the experimental work. Several numerical examples are analyzed in Section 4, along with helpful discussions of imperfect FG beams' tensile, bending, and fatigue tests. Conclusions derived and practical suggestions for future work are outlined in Section 5.

I. Mathematical Formulation

FGM material properties are frequently represented by a power-law function, an exponentially graded form, or a sigmoid function. Consider an FGM beam made of two constituents, as shown in Fig. 1. The volume fraction of the lower part is [27].
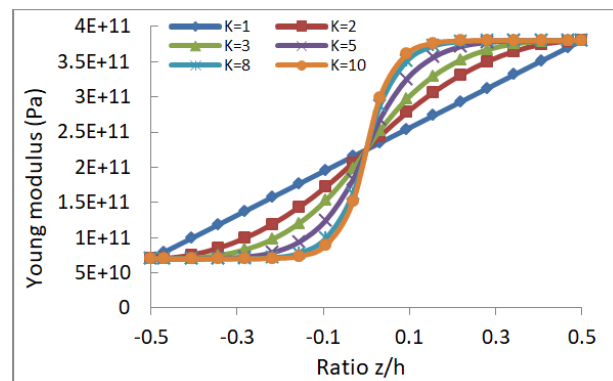
Fig.1. The sigmoid function uses the E (z) behavior change.

$$V_1(z) = \frac{1}{2}\left(\frac{\frac{h}{2}-z}{\frac{h}{2}}\right)^k ; (0 \le z \le \frac{h}{2}) \qquad (1)$$

k represents a volume fraction parameter $[k \le 0 \le \infty]$ representing constituent characteristics through the thickness direction.

From the mixture rule, it can be found that the total volume fraction is:

$$V_1(z) + V_2(z) = 1 \qquad (2)$$

Using the sigmoid formula, it can determine the elastic modulus of the FGM part.

$$E(z) = [1 - V_1(z)]E_2 + V_1(z)E_1 ; [0 \le z \le \frac{h}{2}]$$
$$E(z) = [1 - V_2(z)]E_2 + V_2(z)E_1 ; [-h/2 \le z \le 0] \qquad (3)$$

As seen in Figure 1, the variation in the volume content of (Al/Al$_2$O$_3$) FGM after incorporating various gradient indices k is represented by a sigmoid function.

This study assumes the novel FGVM beam consists of only one metal with an equally distributed porosity volume fraction and graduated through-beam thickness. Accordingly, the sigmoid-law function provides the

following rule for volume fraction [28]:

$$V_p(z) = V_m - \alpha \cdot V_m \cdot \frac{1}{2}\left(\frac{\frac{h}{2}-z}{\frac{h}{2}}\right)^k \qquad (4)$$

For example, if $k = 0$, $V_p(z) = V_m - \alpha\, V_m$, while at $k = \infty$, $V_p = V_m = 1$, where V_p indicates porous metal volume fraction, V_m is the volume of base metal, and α is the porosity parameter. Consequently, the proposed mechanical properties of FGM porous metal can be represented as follows:

$$P(z) = P_m - \alpha \cdot P_m \cdot \frac{1}{2}\left(\frac{\frac{h}{2}-z}{\frac{h}{2}}\right)^k \qquad (5)$$

Here, P_m is the value of the material properties of the metal of the FG beam. Thus, for the homogeneous beam (porosity= 0), the material properties, including the equivalent elastic parameters (Young's modulus (E) and mass density (ρ) of the beam, vary through the thickness with a sigmoid-law function can be given as,

$$E(z) = E_m - E_m\alpha \cdot \frac{1}{2}\left(\frac{\frac{h}{2}-z}{\frac{h}{2}}\right)^k \qquad (6)$$

$$\rho(z) = \rho_m - \rho_m\alpha \cdot \frac{1}{2}\left(\frac{\frac{h}{2}-z}{\frac{h}{2}}\right)^k \qquad (7)$$

Where E_m and ρ_m, respectively, stand for Young's modulus and density of the equivalent single layer.
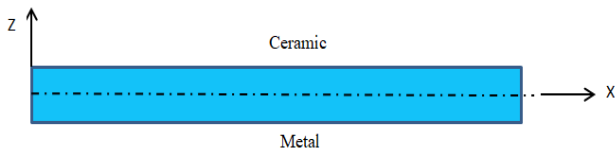

Fig. 1. The Schematic representation of FGVE beam.

1.1. Theoretical Bending Analysis of the FGVM beam

This section examines the static behavior of viscoelastic functionally graded, simply supported beams under bending loads. As a result, bending and shear displacement at the midspan of the sample in a 3-point bending test, the entire deformation (Δ), would be calculated using the equation below [29].

$$\Delta = \Delta_s + \Delta_b = + \frac{Fl}{4(AG)_{eq.}} + \frac{Fl^3}{48(EI)_{eq.}} \qquad (8)$$

(F) is the load associated with the bending, (l) is the span, (A) is the beam's cross-section area, and (G) is the shear modulus.

II. Experimental setup

2.1. Sample Preparation

In this work, various types of additively manufactured (AM), Polytropic acid (PLA), Thermoplastic polyurethane (TPU), Peek 30% CF, and Acrylonitrile–Butadiene–Styrene (ABS), developed by (Zhenjiang Honestar International Trade Co., Limited, China), were employed for 3D printing, with a standard diameter of 1.75 mm. Each type has distinct characteristics and applications that distinguish it from others. Solidworks modeling software was used to create the samples. Tensile, bending, and fatigue tests were performed on the components. Each test involved creating specimens with an even density and products with varying densities over their width. Each test sample was prepared according to standard specifications. Solid Works was used to design the samples. These samples were saved in a (.stl) file, and data was inserted into a 3D printer. A thin wire for the above polymers was used as raw material and fed into 3D printing machines of CR-10 MAX to produce the desired samples. Figure 2a shows the tensile test specimens according to ASTM standard D638. The designed parameters of the printing machine are recorded in Table 1.
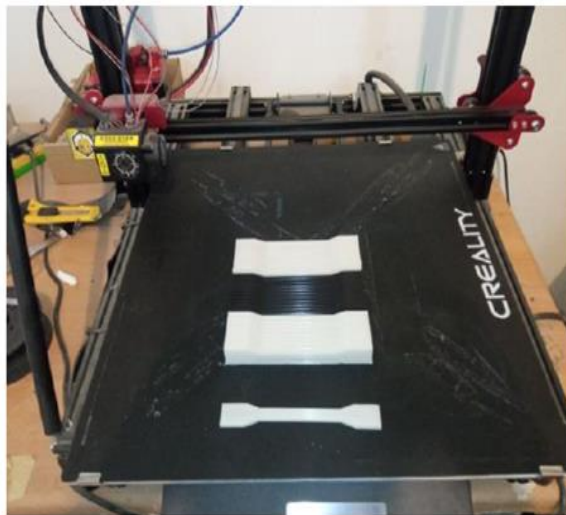
(a)   (b)

Fig. 2. (a) 3D printed polymer tensile test samples following ASTM standard D3763 [30]; (b). Uni-axial tensile experiment.

Table 1.
Printing parameters of all tested samples

| Printing parameters	Value
Nozzle dia.	0.40mm
Layer thickness	0.28mm
Infilling density	100%
Infilling pattern	lines
Printing temp.	200° C
Bed temp.	60° C
Printing speed	50mm/sec.

2.2. Tensile Test

An electronic universal testing machine (UTM) performed uniaxial tensile tests. The loading rate is 2 mm/min, and the preload is 20N. The tensile experiments were carried out on the 3D printed tensile samples according to ASTM standard D638 [30], and the tensile characteristics such as strength and elastic modulus were obtained using strain gauges in the tensile experiment. Because there is no way to determine the exact behavior of polymers through empirical testing, each test takes an average of six readings. Figure 2b displays the stress-strain measurements of the 3D-printed models subjected to tensile loading, and Figure 3 shows the load-displacement curve of ABS samples under tensile load.
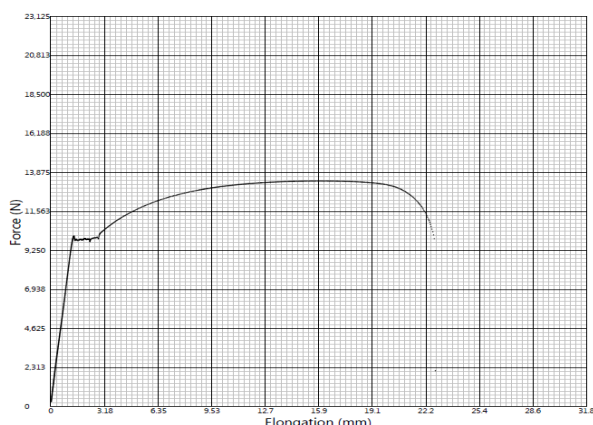
Fig. 3. The force-displacement curves of ABS specimens.

2.3. Three-point bending test

By measuring the flexural strength, strength, and shear modulus of all materials and structures, the three-point bending test is used to evaluate sandwich structures' flexural properties [31]. FG beams are designed and generated using a porosity distribution pattern, which has been one of the main goals of this study. Generally, the pore area's volume fraction follows a power law distribution. 3D printing uses CAD software to generate 3D models of products, or it can scan existing objects [32]. Many materials are used for 3D printing, including thermoplastic polymers such as PLA, ABS, TPU, and others [32]. ASTM Standard D790 [33] was followed to fabricate all polymer specimens with porosity. A 60x10 mm beam with a thickness of 6 mm is used to determine the dimensions and dimensions of the beam. The test uses three values of porosity parameters (0.1, 0.2, and 0.3) and three values of gradient exponents (k = 0.5, 1, and 2). A schematic of the three-point bending test can be seen in Figure 4a, and a representation of the experimental setup can be seen in Figure 4b.
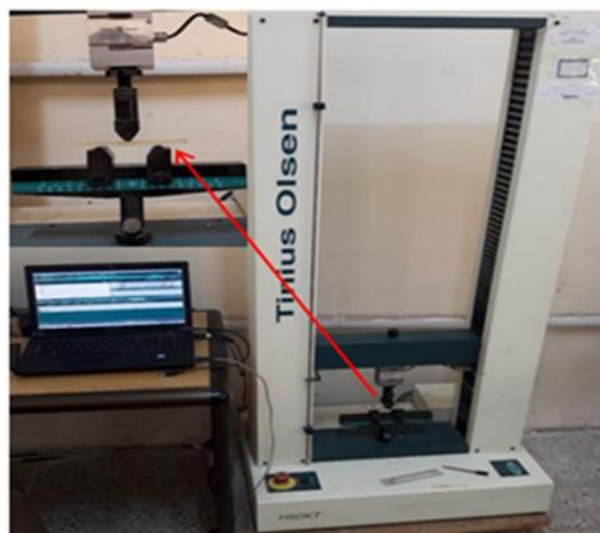
Fig. 4. (a) 3-point bending test configuration according to ASTM D790, (b) Experimental setup for the FG beam.

2.4. Fatigue test

This test was conducted at room temperature under cyclic load and stress ratio (R= -1) using the HI-TECH alternating bending fatigue machine type (HSM20). Figure 5a shows the fatigue standard specimen taken for the analysis according to the standard specification [34], while Figure 5b illustrates the alternating bending fatigue testing machine. Through experiments, the number of cycles to failure was obtained in conjunction with the maximum displacements. This test can generate (S–N) curves of FGM samples, and frequent fatigue life characteristics are evaluated using Basquins law.

The S-N curve can be analytically expressed using Basquin's relation when dealing with finite life (low or high cycle fatigue). It is possible to estimate the material's life with relatively limited information using this technique, as shown in [35]. The stress amplitude (Mpa) can be calculated according to the curve fitting of Basquin's curve:

$$\sigma_a = a \ N_f^b \ \text{(Mpa)} \tag{9}$$

Here, a and b represent constant values depending on the type of material and geometry of the object, while N is the number of cycles to failure. Using the fatigue life estimation equation at 10^6 cycles, we can calculate the fatigue limit using the fatigue life data in the generated S-N curve.

$$\sigma_a = \frac{1.5Et\delta}{l^2} \tag{10}$$

Here, E implies elastic modulus (Gpa), t denotes specimen thickness, δ is displacement obtained by dial gauge (mm), and l is effective length.

III. Numerical investigation

A suitable Finite Element Method (FEM) tool is used [36–39] to validate the results of experimental tests. The current work carried out by the ANSYS 2021 R1 program

(b)   (b)
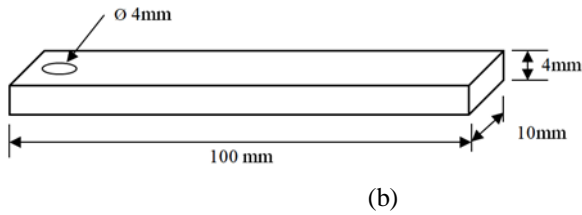
Fig. 5. Fatigue test set up: (a) schematic fatigue specimen, (b) alternating bending fatigue testing machine (HSM20).

is to simulate the 3-point bending and reversed bending fatigue tests on the FG samples with porosities. The FE model proposes two different models, one for bending and the other for fatigue analysis, a gradient arrangement through the beam thickness.

3.1. Simulation of 3-point bending

An analysis of 3-point bending is conducted using a SHELL99 composite element shown in Figure 6. Model boundary conditions were determined after a convergence mesh study had been completed. A gradual load is applied, and simple boundary conditions are used, as shown in Figure 7. For investigating the mechanical performance, four types of viscoelastic materials were examined: acrylonitrile butadiene styrene (ABS), polylactic acid (PLA), Thermoplastic polyurethane (TPU), and PEEK 30% CF. ANSYS' engineering library view incorporates the material characteristics calculated in Equations 6 and 7 for the FE simulation. By employing the results of the experimental work, ABS's general mechanical properties were used, while the standard properties of the other three polymers were given in Table 2. As part of the static structural analysis of the FGVM beam, various parameters are evaluated, including bending load, total deformation, and midspan deflection. A gradient index ($k = 0$ to 25) is also used to calculate the flexural strength of the FGVM beam at different thicknesses.

3.2. Simulation Of Reversed Bending Fatigue Test.

The first decision to be made within the ANSYS fatigue module when performing a fatigue analysis is whether to use the stress or strain life technique. A general analysis with ANSYS involves three steps: creating the geometric model, applying the boundary conditions (loads, supports, etc.), and determining the solution. An ANSYS stress-life analysis was conducted in the present study using ANSYS software. Several options were evaluated for the test conditions. Examples include sample geometry effects, loading mode, stress ratio, and the FG parameters' effect on a structure element's fatigue performance. ANSYS' fatigue module uses a fatigue

model shown in Figure 8.

IV. Results and discussion

4.1. Flexural Bending Test Results

This section examines FGVE beams' performance based on parameters like beam thickness, porosity, and gradient indices. The sample dimensions used are $L = 60$ mm, $W = 10$ mm, and $h = 6$–12 mm, respectively. In addition to 0.1, 0.2, and 0.3 porosity parameters, a gradient index ($k = 0.5, 1, 2$) and three porosity parameters were examined using a UTM. With the help of the testing instrument's PC, we obtained experimental results such as reaction force, applied load, and midspan deflection. Based on the results of experiments using ANSYS software 2021 R1, Figure 10 shows experimental bending data results. The maximum bending load of the model decreases by increasing the importance of the porosity parameter. Fig. 11 shows the same results due to the simulation process by Ansys. A 10% discrepancy was noticed between numerical and experimental bending load results. The technology of 3D printing has proven to be a valuable tool for figuring out how well FGVE structures work mechanically. The midspan deflection of the beam is also illustrated in Figure 12 using experimental results, while Fig. 13 shows the same results based on analysis in Ansy's software. According to numerical results, experimental and ANSYS simulations have a maximum % percentage deflection difference of 9 % for the same FG beam geometrical properties. This percentage influences FG parameters like the power-law index and porous factor.

The results show that the maximum deflection decreases with increasing porosity because of the decrease in material rigidity. One potential source of error is a problem with constructing FG layers in Ansys. Experimental static and dynamic analyses are influenced by noise and system errors. The most common failure mode was yielding, which causes the most deficient specimens. PLA layers with high porosity ratios might also deform the beam due to shear. To better understand
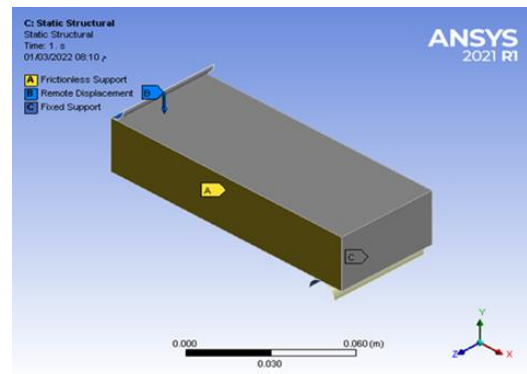
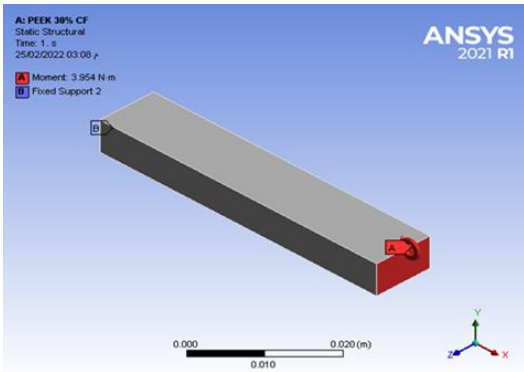**Table 2.**

Materials characteristics used in Ansys [40]

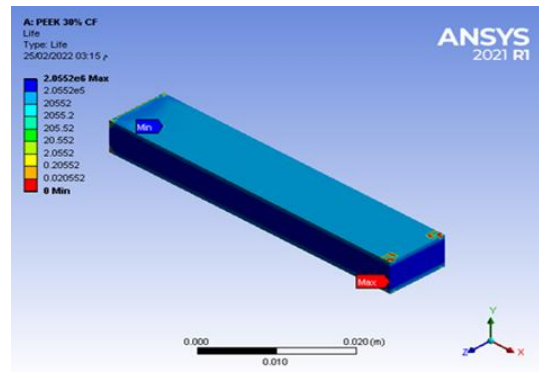| Property	ABS	TPU	PEEK 30% CF	PLA
ρ (kg/m³)	1425	1450	1415	1365
ν	0.40	0.35	0.45	0.35
E (Gpa)	3.56	0.95	7.8	1.45
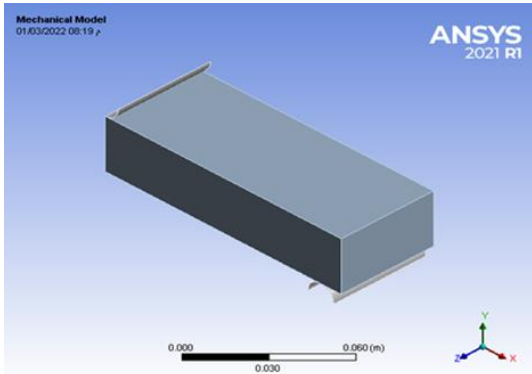
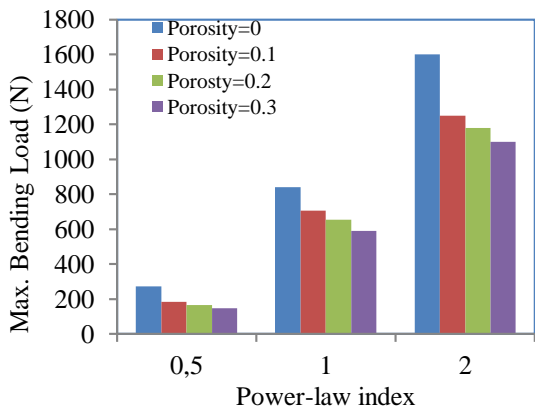**Fig. 6.** The mechanical model in 3-point bending analysis.

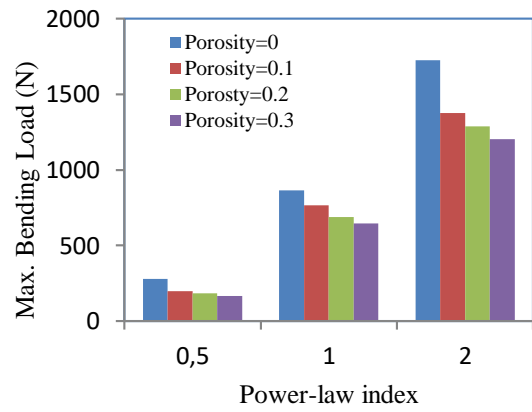**Fig. 7.** The model with BCs in 3-point analysis.

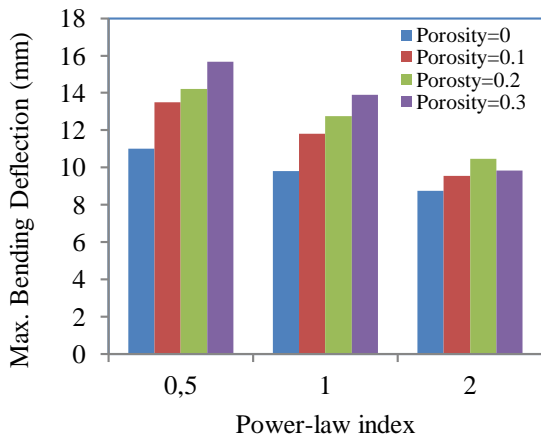**Fig. 8.** The fatigue model generated by Ansys tools.

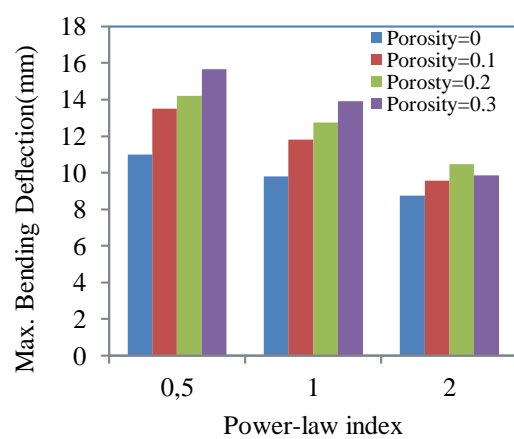**Fig. 9.** Example of fatigue life results.

Fig. 10. The experimental maximum bending load (N) of ABS samples.

Fig. 11. The numerical maximum bending load (N) of ABS samples.

Fig. 12. The experimental maximum bending deflection (mm) of ABS samples.

Fig. 13. The numerical maximum bending deflection (mm) of ABS samples.

the deflection parameter, the following dimensionless deflection parameter ($\overline{w}$) was used [41]:

$$\overline{w} = w\,(x,z).\frac{100E_m bh^3}{Fl^3}. \tag{11}$$

Here, w (x, z) is the maximum deflection, and E_m is Young's modulus of the metal used.

The strain energy of a simply-supported porous ABS beam with different porosity factors (0.1, 0.2, and 0.3), a beam thickness of 6 mm, and by using six values of volume fraction index (k = 0.5, 1, 2, 5, 10, and 25) are numerically shown in Figure 14. It should be noted that the beam made of PEEK 30% CF is preferred in terms of energy absorption due to its higher strength. The strain energy decreases with increasing porosity parameters and gradient index due to decreased material toughness. The deflection parameter similarly yields Figure 15. Compared with ABS, PLA, and TPU, the PEEK beam exhibits the most deflection. Gradually increasing porosity ratios decrease deflection values as material stiffness parameters decrease, causing the deflection values to drop as well. Using backscattered electrons (BSE) and secondary electrons (SE) with a power density of 250 W, a porosity parameter of 0.1, a beam thickness of 6 mm, and a working depth of 1 mm, an ABS-graded sample fractured following the bending test, as shown in figure 16. At the same time, Figure 17 illustrates the SEM image of an ABS sample at 100 μm. No significant striations were found on the fractured surfaces of either sample. However, where local orientations differ, fragmented samples may be at grain or melt pool boundaries. According to the results, FGVM has a very heterogeneous microstructure, and failures most commonly occur from crack initiation and inclusion growth.

4.2. Fatigue results

This study investigates fatigue bending characteristics for rectangular specimens with different porosities and volume fraction indices undergoing completely reversed bending loading. To check the correctness of the experimental work, fatigue analysis using FEA has been conducted using the stress life approach generated by the Ansys tools. Figures 18 to 21 show the observed fatigue life characteristics of ABS polymer samples at three porosity values (0, 0.1, and 0.2) and gradient index k = 0.5, 1, 2, and 5, respectively. There are some trends by comparing those figures; for example, similar behavior in the S-N curve was noticed.

Figures 22 and 23 show the comparison between experimental and numerical fatigue life characteristics of ABS polymer samples at three porosity values of 10% at gradient index k = 5 and 10, respectively. There was no more than a 6% difference in error between the two methods. The results show that FEA simulations can accurately predict the life of materials if the material model and parameters are chosen appropriately. The reliability of this method depends on the consistency of
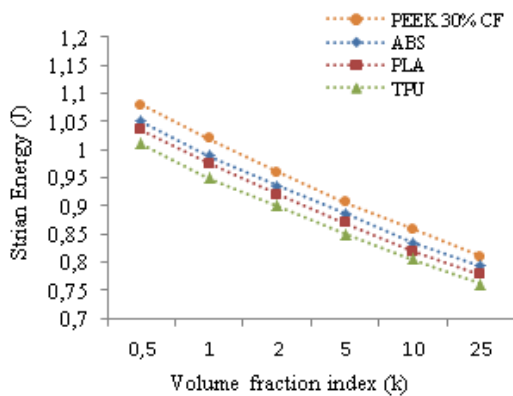

Fig. 14. The strain energy results of a perfect simply-supported beam at various volume fraction indices.
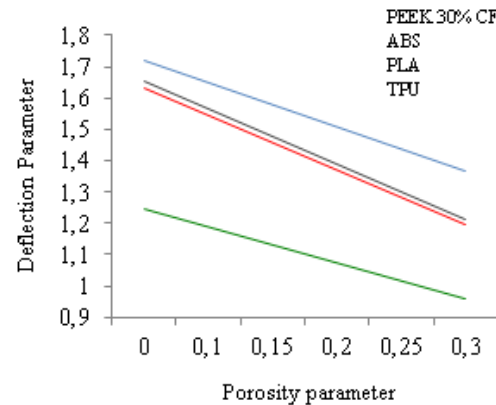

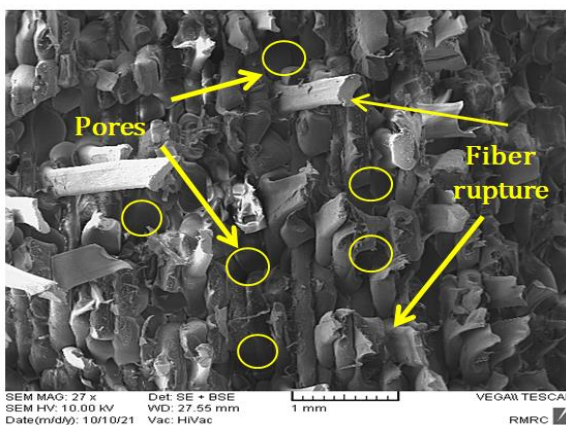**Fig. 15.** Deflection parameters for k = 0.5 and a 10 mm thick beam.

Fig. 16. Image of ABS samples with 0.1 porosity taken by SEM at (1mm).

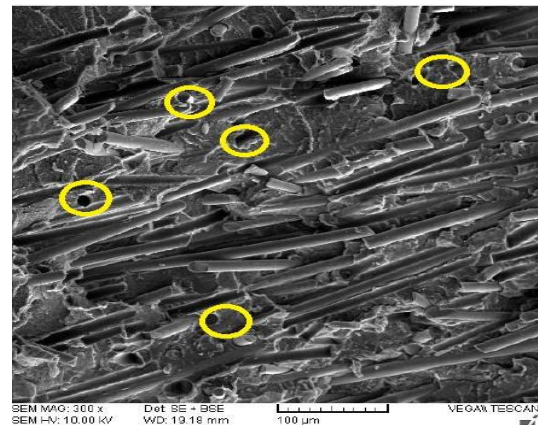**Fig. 17** shows that the SEM viewed ABS samples with 0.1 porosity at (100 μm).

the maximal stress produced by smooth samples and the accuracy of the material total S-N curve generated from experimental results of high cycle fatigue data for rectangular specimens.

Table 3 presents the fatigue life equation at three values of porosity parameters at a power-law index ($k = 1$). For each porosity parameter, 10^6 cycles were

found to be the fatigue limit. This table shows that increasing porosity will decrease the fatigue limit regardless of the type of polymer used. The S-N curve exhibits the following behavior: For all FG polymers, it converges at 0.1 and 0.2, and fatigue life is affected by porosity at low levels. Because of their high strength,
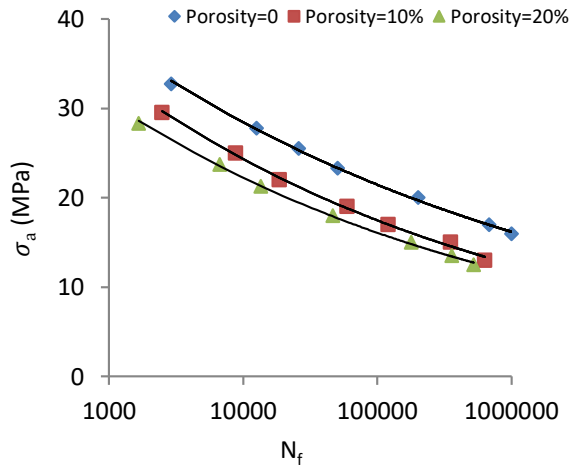
Fig. 18. Experimental S-N curves of different porosity parameters at k=0.5.
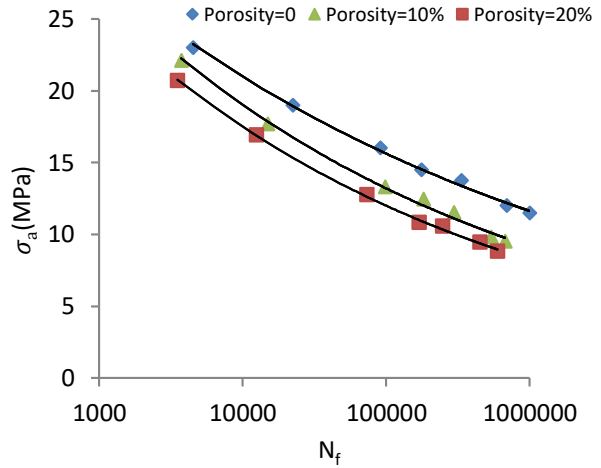
Fig. 19. Experimental S-N curves of other porosity parameters at k=1.
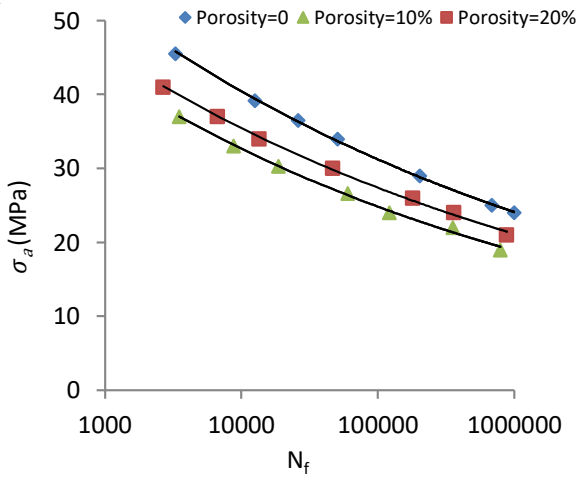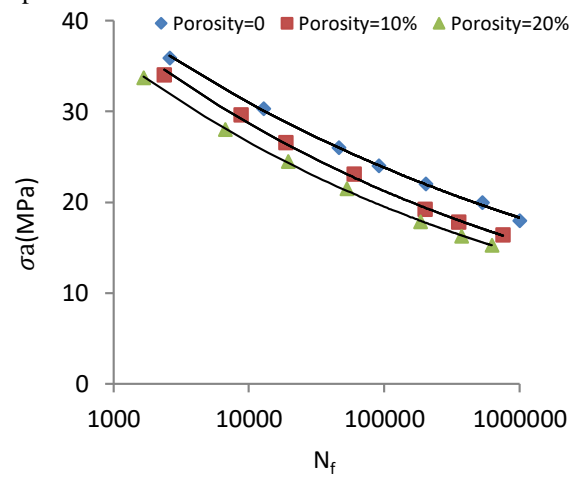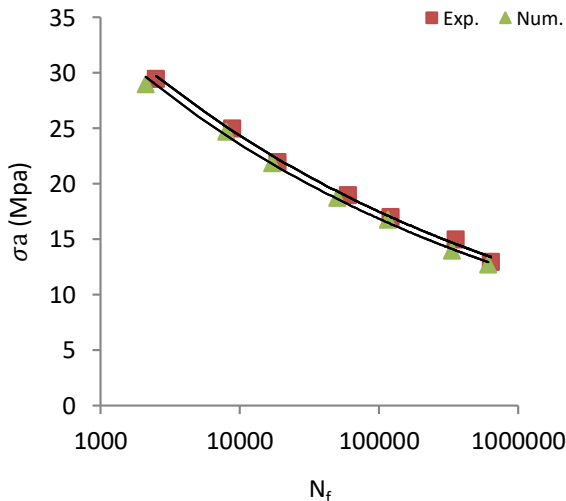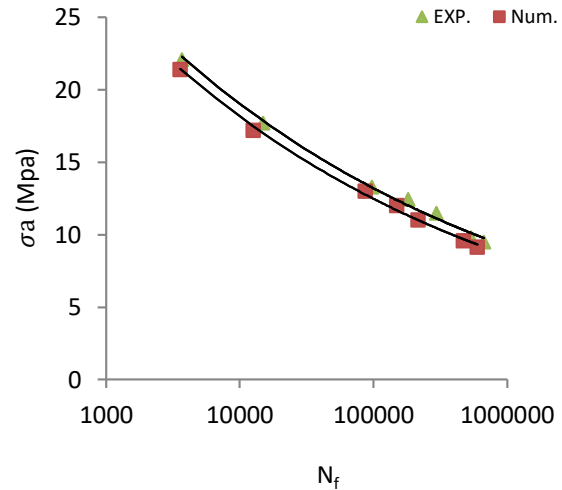

Fig. 20. Experimental S-N curves of different porosity parameters at k=2.

Fig. 21. Experimental S-N curves of different porosity parameters at k=5.

Fig. 22. The numerical and experimental S-N curves at 10% porosity, k =5.

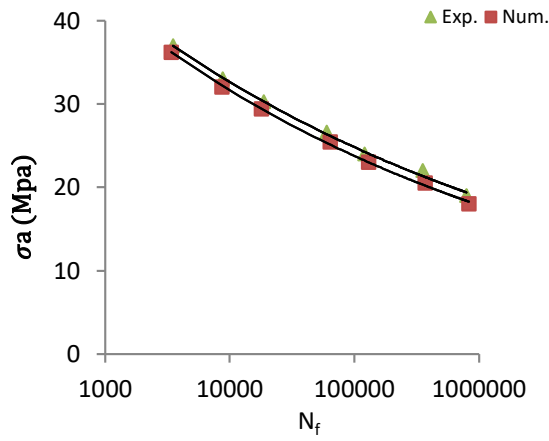**Fig. 23.** The numerical and experimental S-N curves at 10% porosity, k =10.

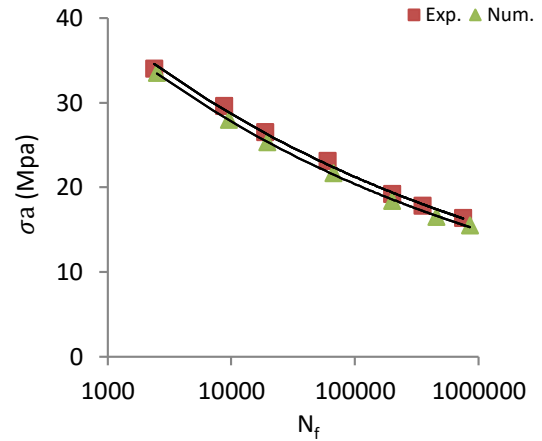**Fig. 24.** The results of S-N curves at 15% porosity, k=1.

Fig. 25. The results of S-N curves at 15% porosity, k=1.

Table 3.

The fatigue life equation results for different porous metals, porosity parameters at (R= -1)

Porous Metal	Porosity parameter	Basequen's Equation	Fatigue limit (Mpa)
PLA	0	$\sigma_L = 87.763N_f^{-0.122}$	16.267
	0.1	$\sigma_L = 91.488N_f^{-0.144}$	12.513
	0.2	$\sigma_L = 81.305N_f^{-0.141}$	11.600
TPU	0	$\sigma_L = 68.378N_f^{-0.128}$	11.665
	0.1	$\sigma_L = 82.007N_f^{-0.159}$	9.117
	0.2	$\sigma_L = 79.276N_f^{-0.164}$	8.225
PEEK 30% CF	0	$\sigma_L = 113.72N_f^{-0.112}$	24.200
	0.1	$\sigma_L = 99.457N_f^{-0.114}$	20.589
	0.2	$\sigma_L = 97.757N_f^{-0.119}$	18.886
ABS	0	$\sigma_L = 88.700N_f^{-0.114}$	18.362
	0.1	$\sigma_L = 95.318N_f^{-0.13}$	15.818
	0.2	$\sigma_L = 91.872N_f^{-0.135}$	14.229

Table 4.

The fatigue limit to tensile strength ratio (σ_f/σ_u)

Polymer type	Stress ratio (R)	(σ_f/σ_u)
TPU	-1	0.390
	- 0.5	0.425
	0	0.525
	0.25	0.537
	0.5	0.615
PLA	-1	0.361
	- 0.5	0.415
	0	0.508
	0.25	0.522
	0.5	0.589
PEEK 30%CF	-1	0.250
	- 0.5	0.288
	0	0.327
	0.25	0.432
	0.5	0.465

PEEK (30% CF) polymers show higher fatigue limits than other types. Both ABS and PLA are porous polymers with similar fatigue life data.

Table 4 presents the fatigue limit to tensile strength ratio (σ_L/σ_u) calculated for five values of stress ratio (R= - 1, - 0.5, 0, 0.25, and 0.5) at the power-law index k=1, using numerical simulation of perfect samples based on Soderberg theory. According to the findings, this ratio increases with increasing stress ratio, and the TPU samples exhibit more ductility than PLA and PEEK samples. Also, from the results, one can conclude that porosity changes more than other Polymer type less

influence TPU samples. Furthermore, it is seen that there are no significant changes in cycles to failure for PLA and TPU samples and at low values of alternating stresses when changing porosity from 0.1 to 0.2.

Conclusions

The voids and pores are considered critical structural malfunctions and cause overhaul performance instability. However, to overcome the disadvantages of porosities, functionally graded materials can be used to graduate the mechanical properties of pores parts. To account for the large variety of porous polymeric materials in many engineering applications, a comprehensive investigation of static and fatigue analysis, including different environmental, loading, and FG parameters, was carried out in the present work. FGM samples with varying densities were fabricated using different polymer types. The following are the main conclusions of the research results:

In an experiment, a change in porosity from 0 to 0.3 reduced the experimental bending loads of the ABS polymer by 31.25 percent. However, at $k = 0.5$ and 1, the reductions were 47.5% and 29.76%, respectively.

In all porous FG polymer samples, the fatigue results show a noticeable reduction in the fatigue limit due to increased porosity.

The tables and graphs show that ANSYS and experimental analyses are close. The maximum discrepancy percentage for bending tests is only 10%; for deflection measurements, it is only 9%; and for reversed bending fatigue tests, it is only 6%, showing that FGVE samples can be well manufactured using 3D printing.

In order to determine the most suitable beam dimensions, bending loads, strain energy, weight, and deflection values, it is recommended that the design of experiments (DOE) and response surface methods (RSM) be used. Performance and characteristics will determine multifunctional requirements.

Since FGM is not affected by considerable bending or fatigue stresses, it should be able to be used in applications where extensive bending or fatigue stresses are present. So, the paper gives detailed research on porous FGM polymeric materials and relevant analyses and results that will help with their use in the engineering field.

Emad Kadum Njim –Assistant Prof. Dr. (Applied Mechanics);
Sadiq Emad Sadiq –PhD, Lecturer (Applied Mechanics);
Muhammad Safa Al-Din Tahir –PhD, Lecturer (Applied Mechanics);
Mujtaba A. Flayyih – PhD, Lecturer (Applied Mechanics);
Lazreg Hadji – Prof. Dr. (Applied Mechanics).

[1] M. Al-Waily, H. Raad & E.K. Njim, *Free Vibration Analysis of Sandwich Plate-Reinforced Foam Core Adopting Micro Aluminum Powder*, In Physics and Chemistry of Solid State, 23(4), 659 (2022); https://doi.org/10.15330/pcss.23.4.659-668.

[2] A. Garg, M.-O. Belarbi, H.D. Chalak & A. Chakrabarti, *A review of the analysis of sandwich FGM structures*, In Composite Structures, 258, 113427 (2021) Elsevier BV; https://doi.org/10.1016/j.compstruct.2020.113427.

[3] P.S.Ghatage, V.R. Kar & P.E. Sudhagar, *On the numerical modelling and analysis of multi-directional functionally graded composite structures: A review,* In Composite Structures, 236, 111837(2020) Elsevier BV; https://doi.org/10.1016/j.compstruct.2019.111837.

[4] B. Adhikari, P. Dash & B.N. Singh, (2020). *Buckling analysis of porous FGM sandwich plates under various types nonuniform edge compression based on higher order shear deformation theory*, In Composite Structures 251, 112597(2020) Elsevier BV; https://doi.org/10.1016/j.compstruct.2020.112597

[5] K.N. Emad, H.S. Bakhy, and M. Al-Waily, *Analytical and Numerical Investigation of Buckling Behavior of Functionally Graded Sandwich Plate with Porous Core*, Journal of Applied Science and Engineering, 25(2), 339 (2022); http://dx.doi.org/10.6180/jase.202204_25(2).0010.

[6] M. Dhuria, N. Grover & K. Goyal, *Influence of porosity distribution on static and buckling responses of porous functionally graded plates,* In Structures, 34, 1458 (2021) Elsevier BV; https://doi.org/10.1016/j.istruc.2021.08.050.

[7] N. Movahedi, M. Vesenjak, L. Krstulović-Opara, I.V. Belova, G.E. Murch, & T. Fiedler, (2021). *Dynamic compression of functionally-graded metal syntactic foams*, In Composite Structures, 261, 113308 (2021) Elsevier BV; https://doi.org/10.1016/j.compstruct.2020.113308.

[8] Z. Yin, H. Gao, & G. Lin, *Bending and free vibration analysis of functionally graded plates made of porous materials according to a novel the semi-analytical method*, In Engineering Analysis with Boundary Elements 133, 185(2021) Elsevier BV; https://doi.org/10.1016/j.enganabound.2021.09.006.

[9] A.J. Ariza Gomez, M. Caire, L.C.A.R. Torres & M.A. Vaz, *Bend stiffener linear viscoelastic thermo-mechanical analysis. Part I - Experimental characterization and mathematical formulation*, In Marine Structures 77, 102946 (2021) Elsevier BV; https://doi.org/10.1016/j.marstruc.2021.102946.

[10] M. Lezgy-Nazargah, P. Vidal, & O. Polit, *An efficient finite element model for static and dynamic analyses of functionally graded piezoelectric beams.* In Composite Structures, 104, 71 (2013) Elsevier BV. https://doi.org/10.1016/j.compstruct.2013.04.010.

[11] M. Li, C. Guedes Soares & R. Yan, *A novel shear deformation theory for static analysis of functionally graded plates.* In Composite Structures, 250, 112559 (2020) Elsevier BV; https://doi.org/10.1016/j.compstruct.2020.112559.

[12] J.P. Pascon, *Large deformation analysis of functionally graded visco-hyperelastic materials*, In Computers & Structures, 206, 90 (2018) Elsevier BV; https://doi.org/10.1016/j.compstruc.2018.06.001.

[13] Q. Zang, J. Liu, W. Ye, F. Yang, C. Hao & G. Lin, *Static and free vibration analyses of functionally graded plates based on an isogeometric scaled boundary finite element method*. In Composite Structures, 288, 115398 (2022) Elsevier BV; https://doi.org/10.1016/j.compstruct.2022.115398.

[14] S.V. Kuteneva, S.V. Gladkovsky, D.I. Vichuzhanin, & P.D. Nedzvetsky, *Microstructure and properties of layered metal/rubber composites subjected to cyclic and impact loading,* In Composite Structures, 285, 115078 (2022) Elsevier BV; https://doi.org/10.1016/j.compstruct.2021.115078.

[15] S. Chen, B. Tai, & J. Wang, *An experimental study of 3D printing based viscoelastic bimaterial subjected to low-velocity impact*, In Mechanics of Materials, 176, 104508 (2023), Elsevier BV; https://doi.org/10.1016/j.mechmat.2022.104508.

[16] K. Koutoati, F. Mohri, E.M. Daya, & E. Carrera, *A finite element approach for the static and vibration analyses of functionally graded material viscoelastic sandwich beams with nonlinear material behavior*, In Composite Structures, 274, 114315 (2021) Elsevier BV; https://doi.org/10.1016/j.compstruct.2021.114315.

[17] A.M. Zenkour, M.N.M Allam, & M. Sobhy, *Bending analysis of FG viscoelastic sandwich beams with elastic cores resting on Pasternak's elastic foundations*, In Acta Mechanica, 212(3–4), 233 (2009) Springer Science and Business Media LLC; https://doi.org/10.1007/s00707-009-0252-6.

[18] F.I. Stepanov, & E.V. Torskaya, *Modeling of Fatigue Wear of Viscoelastic Coatings*, In Materials, 14(21), 6513 (2021) MDPI AG; https://doi.org/10.3390/ma14216513.

[19] J.P. Pascon, *Large deformation analysis of functionally graded visco-hyperelastic materials*. In Computers & Structures, 206, 90 (2018) Elsevier BV; https://doi.org/10.1016/j.compstruc.2018.06.001.

[20] S.-Q. Zhang, Z.-T. Huang, Y.-F. Zhao, S.-S. Ying, & S.-Y. Ma, *Static and dynamic analyses of FGPM cylindrical shells with quadratic thermal gradient distribution*, In Composite Structure, 277, 114658 (2021) Elsevier BV; https://doi.org/10.1016/j.compstruct.2021.114658.

[21] P. Van Vinh, *Static bending analysis of functionally graded sandwich beams using a novel mixed beam element based on first-order shear deformation theory*, In Forces in Mechanics, 4, 100039 (2021) Elsevier BV; https://doi.org/10.1016/j.finmec.2021.100039.

[22] Q.-H. Pham, & P.-C. Nguyen, *Dynamic stability analysis of porous functionally graded microplates using a refined isogeometric approach*. In Composite Structures, 284, 115086 (2022) Elsevier BV; https://doi.org/10.1016/j.compstruct.2021.115086.

[23] L. Wang, Y. Liu, Y. Zhou, & F. Yang, *Static and dynamic analysis of thin functionally graded shell with in-plane material inhomogeneity*, In International Journal of Mechanical Sciences, 193, 106165 (2021) Elsevier BV; https://doi.org/10.1016/j.ijmecsci.2020.106165.

[24] S.Dastjerdi, B. Akgöz, & Ö. Civalek, V*iscoelasticity in Large Deformation Analysis of Hyperelastic Structures*, In Materials, 15(23), 8425 (2022) MDPI AG; https://doi.org/10.3390/ma15238425.

[25] R. Edouard, H. Chibane, & D. Cavallucci, *New characterizing method of a 3D parametric lattice structure*. In FME Transactions, 49(4), 894 (2021) Centre for Evaluation in Education and Science (CEON/CEES); https://doi.org/10.5937/fme2104894e

[26] Z.M.R. Al-Hadrayi, A.N. Al-Khazraji, & A.A. Shandookh, *Investigation of Fatigue Behavior for Al/Zn Functionally Graded Material*, In Materials Science Forum, 1079, 49 (2022); https://doi.org/10.4028/p-8umjs.

[27] K.N. Emad, H.S. Bakhy, and M. Al-Waily, *Analytical and numerical free vibration analysis of porous functionally graded materials (FGPMs) sandwich plate using Rayleigh-Ritz method*, Archives of Materials Science and Engineering, 110(1), 27 (2021); https://doi.org/10.5604/01.3001.0015.3593.

[28] E.K. Njim, S.H. Bakhy, & M. Al-Waily, *Analytical and Numerical Investigation of Free Vibration Behavior for Sandwich Plate with Functionally Graded Porous Metal Core*, In Pertanika Journal of Science and Technology, 29(3), (2021); https://doi.org/10.47836/pjst.29.3.39.

[29] A.F. Ávila, *Failure mode investigation of sandwich beams with functionally graded core*, In Composite Structures, 81(3), 323 (2007) Elsevier BV; https://doi.org/10.1016/j.compstruct.2006.08.030.

[30] ASTM D638: standard test method for tensile properties of plastics, Annual Book of ASTM Standards, American Society of Testing and Materials, West Conshohocken, 2014.

[31] E.K. Njim, S.H. Bakhy, & M. Al-Waily, *Experimental and numerical flexural analysis of porous functionally graded beams reinforced by (Al/Al$_2$O$_3$) nanoparticles*, International Journal of Nanoelectronics and Materials, 15, 91-106 (2022).

[32] C. Tang, J. Liu, Y. Yang, Y. Liu, S. Jiang, & W. Hao, *Effect of process parameters on mechanical properties of 3D printed PLA lattice structures*. In Composites Part C: Open Access, 3, 100076 (2020) Elsevier BV; https://doi.org/10.1016/j.jcomc.2020.10007.

[33] ASTM D790: Standard test methods for flexural properties of unreinforced and reinforced plastics and electrical insulating materials, *ASTM International*, West Conshohocken, Pa, United States, 2014.

[34] N. P. Roberts, and Nigel R. Hart: Alternating Bending Fatigue Machine (HSM20), *Instruction Manual, Hi-Tech Ltd*. UK., 2001.

[35] J. K. Oleiwi, N. D. Fahad, M. M. Abdulridha, et al., *Laser Treatment Effect on Fatigue Characterizations for Steel Alloy Beam Coated with Nanoparticles*, International Journal of Nanoelectronics and Materials, 16, 105-119, (2023)*.*

[36] E. K. Njim, S. H. Bakhy, M. Al-Waily, *Free vibration analysis of imperfect functionally graded sandwich plates: analytical and experimental investigation*, Archives of Materials Science and Engineering, 111(2), 49 (2021); https://doi.org/10.5604/01.3001.0015.5805.

[37] S.A. Deepak, & R.A. Shetty, *Static and free vibration analysis of functionally graded rectangular plates using ANSYS*, In Materials Today: Proceedings, 45, 415 (2021), Elsevier BV; https://doi.org/10.1016/j.matpr.2020.12.761.

[38] A. Sahu, N. Pradhan, & S.K. Sarangi, *Static and Dynamic Analysis of Smart Functionally Graded Beams*. In Materials Today: Proceedings, 24, 1618(2020) Elsevier BV; https://doi.org/10.1016/j.matpr.2020.04.483.

[39] E.K. Njim, S.H. Bakhy, M. Al-Waily, *Analytical and numerical flexural properties of polymeric porous functionally graded (PFGM) sandwich beams,* Journal of Achievements in Materials and Manufacturing Engineering, 110 (1), 5-15 (2022); https://doi.org/10.5604/01.3001.0015.7026.

[40] F.K. Arndt, and M.D. Lechner, Polymer Solids and Polymer Melts–Mechanical and Thermomechanical Properties of Polymers, Springer-Verlag Berlin Heidelberg, 6A3 2014.

[41] M.D. Do, M.T. Tran, & H.C. Truong, *Bending Analysis of Sandwich Beam with Functionally Graded Face Sheets Using Various Beam Theories by Meshfree Method*, In Kalpa Publications in Engineering. Proceedings of International Symposium on Applied Science 3, 139-149 (2020); https://doi.org/10.29007/9nvf.

Е.К. Нджім[1], С.Е. Садік[2], М.С. Аль-Дін Тагір[3], М.А. Флайїх[4], Л. Хаджь[5]

Аналіз згину, вигину та зношення функціонально градуйованих в'язкопружних матеріалів: експериментальний та чисельний підходи

[1]*Міністерство промисловості та корисних копалин, Державна компанія гумової та шинної промисловості, Ірак, emad.njim@gmail.com;*
[2]*Технічний університет Аль-Фурат Аль-Аусат, Ірак;*
[3]*Університет Імама Джафара Аль-Садіка, Ірак;*
[4]*Університет Аль-Мустакбал, Хілла, Вавилон, Ірак;*
[5]*Університет Тіарет, Тіарет, Алжир*

У роботі синтезовано термопластичний полімер із змінною щільністю в одному напрямку за допомогою технології адитивного виробництва для вивчення динамічних і статичних характеристик функціонально градуйованих в'язкопружних матеріалів (FGVM). Для опису механічних властивостей FGVM було запропоновано аналітичне формулювання, засноване на формулюванні сигмоподібного закону. Експериментальну частину виконували на зразках, надрукованих 3D-друком, виконуючи різні випробування, щоб перевірити ефективність таких матеріалів. Крім того, для оцінки властивостей конструкції на вигин застосовано метод скінченних елементів. Детально проаналізовано вплив параметрів FG та геометричних властивостей на тривалість навантаження при згині та зворотному вигині. Результати показують, що збільшення пористості з 10% до 30% при степеневому індексі (k = 2) зменшує міцність на вигин на 31,25 відсотка та прогин приблизно на 11,2 відсотка для зразків VE. Зміна показника степеневого закону від 0,5 до 10 збільшує витримку на міцність на 35 %.

Ключові слова: полімерні матеріали, механічні характеристики, зношення.